Results of Temperature-Dependent LiPB Cell Modeling for HEV SOC Estimation

Gregory L. Plett

Abstract

The ability to estimate state-of-charge (SOC) is a critical requirement of any battery management system for HEV/BEV application. For a practical implementation, the estimate must be accurate over the entire operating range of the pack; in particular, over the entire automotive temperature range.

In previous papers, we have described how to estimate SOC using Kalman filtering methods. These algorithms depend on a mathematical model of cell dynamics; the better the model, the better the SOC estimation. In this paper, we describe how to extend our previous work to model cell dynamics over a wide range of temperatures. Results are presented. *Copyright*$^{©}$ *2005 EVS21*

Keywords: Modeling, battery model, battery management, lithium polymer, state of charge.

1. Introduction

In previous papers [1–6] we have proposed methods for cell SOC estimation that use an algorithm based on extended Kalman filtering (EKF). EKF requires a mathematical model of cell dynamics able to predict cell electrical behavior. An SOC estimate is updated based on the difference between model prediction and measured data. We have been able to achieve very good estimation using proto-type high-power LiPB HEV cells.

The previously reported results were based on experiments conducted at room temperature (25ºC), and used a cell model optimized for room-temperature modeling of cell dynamics. In order for the method to be useful in practice, however, it must work over the entire anticipated cell operating range; particularly, it must work over the entire automotive temperature range.

Cell dynamics vary sufficiently with temperature that a single cell model optimized for room-temperature operation fails to allow good SOC estimation via EKF over the –30ºC to 50ºC range, for example. Fortunately, it is possible to remedy this situation, which is the topic of this paper.

We proceed by first reviewing the cell model used in previous work for room-temperature applica-tion. We then show how it may be generalized to other temperatures by first considering open-circuit-voltage (OCV) effects, and then the effects on other parameters. Then, we describe how we used cell-test data to fit values to the generalized model, give modeling results and SOC-estimation results. Finally, the results are evaluated and conclusions made.

2. Review of the Enhanced Self Correcting (ESC) Cell Model

In order to use EKF to estimate SOC, we require an electrical input-output model of the behavior of the electrochemical cells being used; in our case, a Lithium Ion Polymer Battery (LiPB) technology. The cells are treated as nonlinear dynamic systems, represented in a discrete-time state-space form. We assume the form

$$x_{k+1} = f(x_k, u_k) + w_k \tag{1}$$
$$y_k = g(x_k, u_k) + v_k, \tag{2}$$

where x_k is the system state vector at discrete-time index k, u_k is the measured exogenous system input at time k (which may include measurements of battery-pack current, temperature and so forth) and w_k is unmeasured "process noise" affecting the system state (and also models the inaccuracy of the cell model, to some extent). The system output is y_k, and v_k is the measurement noise that usually models noise in sensors. Equation (1) is called the "state equation", (2) is called the "output equation", and $f(\ )$ and $g(\ )$ are (possibly nonlinear) functions, specified by the particular cell model used.

To be more specific, the system input vector u_k typically contains the instantaneous cell current i_k. It may also contain the cell temperature T_k, an estimate of the cell's capacity C, and/or an estimate of the cell's internal resistance R_k, for example. The system output is typically a scalar but may be vector valued as well. Here we consider the output to be the cell's loaded terminal voltage—not at-rest open-circuit-voltage (OCV). The system's state vector x_k in some way represents in summary form the total effect of all past input to the system so that the present output may be predicted solely as a function of the state and present input. Values of past inputs are not required. Our method constrains the state vector to include SOC as one component, so that SOC may later be estimated using EKF.

Many cell models have been proposed in the literature for many purposes. The specific application we have in mind is to model cell dynamics for the purpose of state-of-charge estimation in a hybrid electric vehicle (HEV) battery pack. The HEV application is a very harsh environment with rate requirements up to about ±40C, very dynamic rate profiles, and operating temperatures between –30ºC and 50ºC. This is in contrast to relatively benign portable-electronic applications with constant power output and fractional C rates. Methods for cell modeling and SOC estimation that work well in portable electronic devices often fail in the HEV application. If precise SOC estimation is required by the HEV, then a very accurate cell model is necessary.

The model that we use as our baseline in this paper is one that we have called the "enhanced self-correcting" (ESC) cell model [3,5]. In order to use the Kalman methods we propose to estimate SOC, the cell model must be represented in the discrete-time state-space form of (1) and (2) with the constraint that SOC is a member of the state vector. The difference between the models, then, depends only on the definitions of x_k, u_k, $f(\ )$ and $g(\ )$.

The basis for the SOC state-equation is developed as follows: If $z(t) = \text{SOC}$, we know that

$$z(t) = z(0) - \int_0^t \frac{\eta(i(\tau))\,i(\tau)}{C}\,d\tau, \tag{3}$$

where C is the nominal capacity of the cell, $i(t)$ is the cell current at time t, and $\eta(i(t))$ is the Coulombic efficiency of the cell. A discrete-time approximate recurrence may then be written as

$$z_{k+1} = z_k - \frac{\eta(i_k)\,i_k\,\Delta t}{C}, \tag{4}$$

where Δt is the sampling period (in hours). Equation (4) is used to include SOC in the state vector of the cell model as it is in state equation format already, with SOC as the state and i_k as the input.

The dynamics of the change of polarization voltage are also captured by a state equation. We add "filter states" with linear dynamics:

$$\left[f_{k+1}\right] = \left[\text{diag}(\alpha)\right]\left[f_k\right] + i_k. \tag{4}$$

The vector α has N filter "poles", with $|\alpha| < 1$ for stability, corresponding to time constants of the polarization voltage dynamics. A value of $N \approx 4$ works well.

A further phenomenon captured by a state equation is that of hysteresis. A cell that has recently undergone a charge event will have a higher rest voltage than one that has undergone a discharge event, even at the same SOC. That is, voltage does not decay to OCV, but to OCV plus/minus a factor based on the hysteresis of the cell. We note that hysteresis is not a phenomenon generally associated with lithium-ion systems, since most applications have been in the light portable electronics area where SOC accuracy is not as critical as in the HEV application and where temperatures are not as extreme. It is, however, very pronounced at low temperatures and can lead to SOC errors as large as ±40% if the estimate is based simply on OCV (even with full cell relaxation), particularly with Mn/graphite-based chemistries. The reason is the spread between the charge and discharge characteristics coupled with the flat nature of the curves between 10% and 90% SOC.

A hysteresis state implementing a linear-time-varying difference equation may be modeled as:

$$h_{k+1} = \exp\left(-\left|\frac{\eta(i_k)i_k\gamma\Delta t}{C}\right|\right)h_k + \left(1 - \exp\left(-\left|\frac{\eta(i_k)i_k\gamma\Delta t}{C}\right|\right)\right)M(z,\dot{z}). \tag{5}$$

$M(z,\dot{z})$ is a static function representing the maximum hysteresis at the present SOC and rate-of-change of SOC, and γ is a hysteresis rate constant

The three components of the system state are combined, resulting in

$$x_k = \begin{bmatrix} f_k^T & h_k & z_k \end{bmatrix}^T. \tag{6}$$

The corresponding equations for f_k, h_k, and z_k then combine to form the vector function $f(\ )$.

The cell terminal voltage is modeled by the output equation $g(\ )$. With the states of the system as defined, the ESC model computes:

$$y_k = \text{OCV}(z_k) + C[f_k] - Ri_k + h_k. \tag{7}$$

The voltage is computed as the sum of the open-circuit-voltage at the present SOC, plus a weighted sum of the polarization voltage states, minus ohmic losses, plus hysteresis. A further constraint on (7) ist hat during a constant-current dis/charge, the polarization filter voltages must converge to zero so that $y_k \rightarrow \text{OCV(SOC)} - I \times R$ (plus hysteresis). This constraint is satisfied if the filter has zero dc gain [5], which may be enforced in the filter design.

The form of the ESC model is now completely described. In order to implement the model for a specific cell electrochemistry, however, we require knowledge of the parameters of the model. Specifically, we must determine the OCV versus SOC relationship, the filter time constants α, the number of filter states N, hysteresis rate factors, and so forth. In the following sections, we describe how this was done for our prototype cells, and some modeling results.

3. Modeling OCV; cell tests to model OCV

In this section, we describe cell tests performed to gather OCV data, how the data was analyzed, and the resulting form of equations that predict OCV for our cells at different temperatures. Note that the cells used in this paper differ electrochemically from those reported in previous work [1–7]. We refer to the older cells as GEN3 cells, and to the newer cells as G4 cells. The GEN3 cells are high-power (>20C capable) 7.5Ah Mn spinel/graphite LiPB, and the G4 cells are very high power (>30C capable) 5Ah Mn spinel/blended-carbon LiPB, both reported in [8].

Several steps are required to generate a good temperature-dependent model of G4 cell OCV characteristics. First, we conducted OCV tests at the following temperatures: –30, –20, –10, 0, 10, 20, 30, 40 and 50 degrees Celsius to collect raw data. Three G4 cells were connected in parallel (to electri-

cally average their responses) resulting in a "super-cell" with nominal capacity of about 15 Ah. The following procedure was conducted each time (using an Arbin BT2000 cycler and a Tenny thermal chamber):

1. Soak super-cell at 25ºC for at least 2 hours.
2. Charge the super-cell: CC @ 1C (15A) to 4.2V, CV @ 4.2V to 0.01A.
3. Soak the super-cell at the test temperature for 2 hours.
4. Discharge the super-cell CC @ C/30 (0.5A) until voltage equal to 2.5V.
5. Rest for 30 seconds.
6. Charge the super-cell CC @ C/30 (0.5A) until voltage equal to 4.2V.

Data points were collected periodically, including voltage, Ah discharged and Ah charged.

Secondly, a preliminary OCV versus SOC relationship was estimated at each temperature. SOC during discharge was calculated as 1–(present Ah discharged)/(total Ah discharged). SOC during charge was calculated as (present Ah charged)/(total Ah charged). The discharge curve was plotted as voltage versus SOC discharged, and the charge curve was plotted as voltage versus SOC charged. The preliminary OCV curve for each temperature was estimated by averaging the discharge and charge voltages at each SOC. The averaging process eliminates, to the greatest degree possible, the effects of hysteresis and ohmic polarization voltage. The charging and discharging were done at a slow enough rate to minimally excite polarization voltage time constant dynamics.

The third step combined the different temperature-dependent preliminary OCV curves into one relationship. We store two different functions: one is nominal OCV at 0ºC, and the other is a per-degree correction factor. Therefore, for temperature T (in degrees Celsius), we compute the OCV as:

$$OCV(SOC, T) = OCV0(SOC) + T \times OCVrel(SOC).$$

The two curves OCV0 and OCVrel were found by least-squares fitting all of the temperature-dependent preliminary OCV curves, as computed above. (Note the memory savings by using only two relationships—OCV0 and OCVrel—versus the many relationships that might be required by storing OCV at a plurality of temperatures).

The OCV relationship found in this way works quite well. The least-squares fitting approach helps average out some random test error, and helps give a good OCV curve for the low-temperature region, where the individual curves are not very reliable due to hysteresis effects. However, some imperfections remain. For example, we assume in the cell tests that SOC=0 on discharge when we have reached 2.5V, which is not true at temperatures other than 25ºC. On charge we assume that SOC=1 when we have reached 4.2V, which is again not true at temperatures other than 25ºC. Therefore, there are some small compression/expansion/shifting issues in the curves. A final step is used to help correct this.

First, the enhanced self-correcting (ESC) cell model was fit to dynamic test data using the OCV relationship as found thus far, and as described in the following section. When convergence of the model was achieved, the model parameters were frozen. Average model error versus SOC was found at all temperature test points, and was used to adapt OCV0 and OCVrel in a direction to reduce error. (Least-squares fitting was again used). Adaptation continued until modeling error was not improved. Small (1%–2%) modeling gains were achieved. While the gain is small, it is important because it helps eliminate model bias, and bias is detrimental to EKF-style SOC estimation. The final OCV versus SOC and temperature curves are plotted in Figure 1.
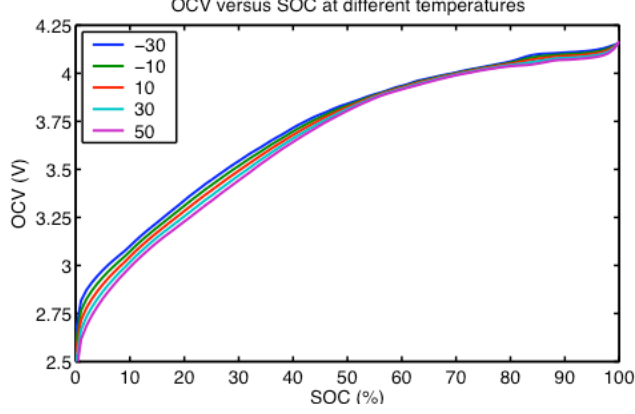
Figure 1: Model of OCV versus SOC at different temperatures.

4. Modeling dynamics; cell tests to model dynamics

In this section, we describe cell tests performed to gather data to be used to fit numeric values to the parameters of the ESC model to explain cell dynamic behavior. The particular form of model generalization is explained, and the method of optimizing numeric values is discussed.

The data comprised tests at –30, –20, –10, 0, 10, 25, 35 and 45 degrees Celsius where sequences of UDDS drive cycles were conducted over the entire SOC range for each test. The UDDS current versus time profile was generated by NREL's ADVISOR program [9], scaled for a small sedan. Each cycle resulted in a slight elevation of SOC, so the test script executed 15A×1.5 min = 0.375 Ah discharges (13% SOC) between cycles so that the overall testing process would spread over the operational SOC range. If any cycle resulted in a voltage outside of the 2.5V to 4.2V range, that particular cycle was aborted, and the script continued to the subsequent discharge and repeat portion of the sequence. The procedure that we followed was:

1. Soak cell at 25ºC for at least 2 hours.
2. Charge the cell: CC @ 1C (5A) to 4.2V, CV @ 4.2V to 0.01A.
3. Soak the cell at the test temperature for 2 hours.
4. Execute the test profile, comprising 22 UDDS cycles separated by discharges and 5 min rests.

Data points were collected periodically, including time, current, voltage, Ah discharged and Ah charged. A representative plot of cell terminal voltage as a function of time is plotted for the room-temperature test in the left frame of Figure 2. In the right frame, a zoomed-in region is shown to magnify detail.

Initial data fitting for an enhanced self-correcting cell model was performed using an optimization procedure and data collected from cells. The model used three filter states, one hysteresis state, and one SOC state, so the set of parameters to be optimized was:

$$\theta = \begin{bmatrix} \eta, & C, & \alpha_1 \cdots \alpha_3, & g_1 \cdots g_2, & \gamma, & R, & M \end{bmatrix}^T.$$

Optimization was initialized by providing a preliminary estimate for θ. The ESC model was then run (open-loop) using cell-test current data as input, and the model output voltage was recorded. After an entire data set was simulated by the ESC model for a particular θ, (*i.e.*, all 22 UDDS cycles, discharges and rests), the root-mean-squared (RMS) difference between simulated model output voltage and measured cell output voltage was used as an indicator of the utility of the parameter set θ. The parameters were modified in a direction to reduce RMS error, and the procedure iterated. When RMS
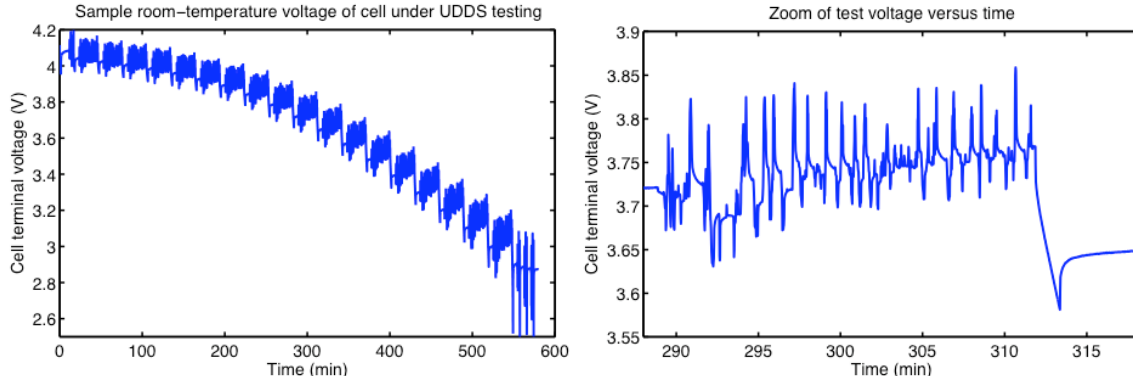
Figure 2: Voltage versus time for a representative cell test for dynamic modeling.

error converged, the optimization was terminated. Optimization was done using Matlab's Optimization Toolbox, although any appropriate method might have been used.

Initial data fitting resulted in eight different sets of parameters—one for each test temperature. In an application, however, the battery-pack temperature would frequently be somewhere between two temperatures from the test cases. We require a method to interpolate parameters between adjacent test cases in order to predict cell behavior at any temperature. Our first idea was to tabulate each parameter as a function of temperature, and use linear interpolation between temperatures in order to select a parameter value. However, we found that the cell-model parameters at one temperature were not necessarily similar to cell-model parameters optimized from cell tests at an adjacent parameter. No smooth curve was able to model every parameter as a function of temperature.

Since we anticipate that true cell dynamics are not discontinuous—that is, that they vary smoothly with temperature—this observation must be due to over-fitting the data when we made separate models for each temperature. Our subsequent approach was to use the eight individually optimized models as a starting point, but to then jointly use all data to fit a smooth curve to each parameter as a function of temperature. We made each parameter a polynomial in temperature (fifth-order seemed to work well), and we optimized the values of the polynomials to best fit all of the data sets. The overall modeling error using this approach was higher than using individual models for each temperature, but the advantage was that each parameter varied smoothly with temperature, and linear interpolation gave good results at temperatures not in the original data set.

RMS modeling errors for GEN3 cells and for G4 cells, at different temperatures, are displayed in Table 1. Note that error was only evaluated over the SOC range 5%–100% due to the apparent extreme nonlinearity of G4 cells below 5% SOC, and the fact that we do not plan to operate the cells in this region. Both generations of cells have equivalent error at –30ºC. The G4 cell is better modeled for –20ºC. The GEN3 cell is better modeled for all other temperatures. A contributing factor, I believe, is that the GEN3 and G4 cells are being exercised at equivalent power levels, but because of their different capacities this results in much higher relative rates for the G4 cell. This in turn stresses the cell to a greater extent, and excites more nonlinear behavior than in the GEN3 counterpart. At the present time, however, the SOC estimation results for G4 are good, as presented in the next section.

6

Table 1: RMS modeling error (mV) for tests at various temperatures (degrees Celsius)

Temp.	–30	–25	–20	–15	–10	–5	0	5	10	15	20	25	30	35	40	45
GEN3	35.4	32.1	37.0	22.6	12.9	7.8	4.3	7.1	4.8	2.5	5.1	4.2	3.9	3.2	2.9	3.2
G4	35.3	—	16.4	—	16.7	—	11.7	—	12.6	—	—	7.3	—	9.9	—	11.8

5. SOC Estimation Results

The critical test for model validation is how well SOC may be estimated using the model. In the past, we have used a type of nonlinear Kalman filter called the *extended Kalman filter* (EKF) to estimate SOC [2,3,6]. Here, we use a variant of the EKF, the details of which are beyond the scope of this paper.

Several test cases are of interest here. First, in Table 2, we give results using this nonlinear Kalman filter for the various test temperatures when the KF was correctly initialized, and when the same data was used to both train the model and test the filter. The first table row gives the maximum absolute SOC error over the test; the second row gives the root-mean-squared error over the test, and the bottom row gives the fraction of time that the bounds do not encompass the correct solution. The maximum absolute error is generally in the 3% ballpark, which is commendable. The RMS error is around 0.5%, which indicates that the error is very infrequently larger than about 1.5%, and the bounds error is generally less than 1%, which indicates that the SOC plus bounds estimates may be used to give very good ranges for the true SOC. For example, SOC plus bounds might be used to compute charging power available, and SOC minus bounds might be used to compute discharge power available [7].

Table 2: Results when testing nonlinear KF using training data and correct initialization.

Temperature	–30ºC	–20ºC	–10ºC	0ºC	10ºC	25ºC	35ºC	45ºC
Max abs error	2.85%	3.18%	2.26%	1.96%	1.56%	1.36%	1.65%	3.09%
RMS error	0.38%	0.37%	0.47%	0.62%	0.40%	0.20%	0.40%	0.51%
Bounds error	0.21%	0%	0%	6.48%	0%	0.44%	0.21%	3.47%

Table 3 gives results when testing the nonlinear KF using the same data used for training the cell model, but with the KF initialized (incorrectly) to a SOC of 80% (instead of the correct initialization of 100%). This case is given as an example of the KF recovering from the initial error and converging to the correct answer despite poor initialization. Other methods (coulomb counting, for example) are unable to recover from an initial bad estimate. In this table, we do not show maximum absolute error, since it is always 20% (from the incorrect initialization). Instead, we show the convergence time of the filter to an estimate that is 2% different from the correct SOC. This convergence time is a function of the tuning parameters of the filter. In general there is a tradeoff between convergence speed and steady-state accuracy. In this case, the filter is tuned for acceptable steady-state accuracy, but convergence time in the order of five to ten minutes. The RMS error after convergence is very similar to the previous case, and the bounds, after convergence, are nearly as good as well.

Tables 4 and 5 are comparable to tables 2 and 3, except that they now use different data to test the cell versus the data used to train the cell model. That is, the test sequence was executed on one cell, and that data was used to optimize a cell model. Then, the same test sequence was run on a different cell from the same production facility (with same electrochemistry, but slightly differing dynamics due to slight variations in manufacture) to see how well the KF could predict the SOC of the different cell. In Table 4, the KF was correctly initialized, and we see that the maximum absolute error is somewhat

Table 3: Results testing nonlinear KF using training data and incorrect initialization.

Temperature	–30ºC	–20ºC	–10ºC	0ºC	10ºC	25ºC	35ºC	45ºC
Converge time (s) to 2%	714	1039	937	289	137	101	471	241
RMS error after converge	0.36%	0.27%	0.38%	0.63%	0.44%	0.30%	0.46%	0.65%
Bounds error	0.93%	0.52%	0.01%	6.52%	0.01%	0.45%	0.25%	3.48%

higher, but still good. The RMS error is noticeably higher, but again still good. The fraction of time that the bounds do not encompass the correct solution is very high, however. Future work must examine ways to improve this metric. Table 5 gives results with the KF incorrectly initialized (to 80% instead of 100%). Convergence time is higher than before, RMS error is somewhat higher than before, and the bounds are again very poor. In the cases of both Tables 4 and 5, the bounds are optimistically small. Wider error bounds would encompass the solution.

Table 4: Results when testing nonlinear KF using testing data and correct initialization.

Temperature	–30ºC	–20ºC	–10ºC	0ºC	10ºC	25ºC	35ºC	45ºC
Max abs error	2.74%	4.99%	2.49%	2.01%	1.57%	2.57%	2.70%	2.43%
RMS error	0.61%	1.01%	0.91%	0.69%	0.41%	1.60%	1.36%	0.64%
Bounds error	61.52%	53.00%	57.54%	9.24%	0%	73.15%	84.53%	25.16%

Table 5: Results testing nonlinear KF using testing data and incorrect initialization.

Temperature	–30ºC	–20ºC	–10ºC	0ºC	10ºC	25ºC	35ºC	45ºC
Converge time (s) to 2%	416	2055	1071	303	137	339	652	246
RMS error after converge	0.60%	0.94%	0.85%	0.69%	0.44%	1.64%	1.43%	0.75%
Bounds error	63.05%	54.71%	55.61%	8.93%	0.01%	73.16%	87.21%	24.86%

6. Conclusions

We have presented the method with which the G4 OCV relationship is determined and modeled, results from ESC model fitting, and SOC estimation using a nonlinear Kalman filter. While the new cells are not fit as well as the old cells using the ESC model, SOC estimation is still quite good. There appears to be a tradeoff: the new cells are being exercised at higher relative rates, which makes modeling more difficult. On the other hand, the OCV relationship is much steeper, making SOC estimation more accurate. Future work must focus on improving the error bounds, and on generalizing from a training cell to test cell.

References

[1] Plett, G., "LiPB dynamic cell models for Kalman-filter SOC estimation," in *CD-ROM Proceedings of the 19th International Battery, Hybrid and Fuel Cell Electric Vehicle Symposium & Exhibition (EVS19),* (October 2002), Busan, Korea.

[2] Plett, G., "Kalman-Filter SOC Estimation for LiPB HEV Cells," *Proceedings of the 19th International Battery, Hybrid and Fuel Cell Electric Vehicle Symposium & Exhibition (EVS19),* (October 2002), Busan, Korea.

[3] Plett, G., "Advances in EKF LiPB SOC Estimation," in *CD-ROM Proceedings of the 20th Electric Vehicle Symposium (EVS20),* Long Beach CA, (November 2003).

[4] Plett, G., "Extended Kalman Filtering for Battery Management Systems of LiPB-Based HEV Battery

Packs―Part 1: Background," *Journal of Power Sources*, Vol. 134, No. 2, August 2004, pp. 252–61.

[5]   Plett, G., "Extended Kalman Filtering for Battery Management Systems of LiPB-Based HEV Battery Packs―Part 2: Modeling and Identification," *Journal of Power Sources*, Vol. 134, No. 2, August 2004, pp. 262–76.

[6]   Plett, G., "Extended Kalman Filtering for Battery Management Systems of LiPB-Based HEV Battery Packs―Part 3: State and Parameter Estimation," *Journal of Power Sources*, Vol. 134, No. 2, August 2004, pp. 277–92.

[7]   Plett, G., "High-Performance Battery-Pack Power Estimation Using a Dynamic Cell Model," *IEEE Transactions on Vehicular Technology*, Vol. 53, No. 5, September 2004, pp. 1586–93.

[8]   Kim, S.W., Yu, J.S. Namgoong, J. Kim, J.H., Kim, M.H., "Progress in Li-ion Polymer Battery and Pack System of LG Chem. For Transportation Applications," in *CD-ROM Proceedings of the 20th Electric Vehicle Symposium (EVS20),* Long Beach CA, (November 2003).

[9]   CTTS Vehicle Systems Analysis Homepage, http://www.ctts.nrel.gov/analysis/, accessed May 2003.

Author

Dr. Gregory L. Plett, *Assistant Professor,*
Dept. of Electrical and Computer Engineering, University of Colorado at Colorado Springs,
1420 Austin Bluffs Parkway, P.O. Box 7150, Colorado Springs, CO 80933–7150 USA
Tel: +1–719–262–3468, Fax: +1–719–262–3589, E-mail: glp@eas.uccs.edu,
URL: http://mocha-java.uccs.edu, *and consultant to*
Compact Power Inc., 1200 S. Synthes Ave., Monument, CO 80132 USA
Tel: +1–719–488–1600x134, Fax: +1–719–487–9485, E-mail: gplett@compactpower.com.
URL: http://www.compactpower.com/.